Nanoscale Research Letters

RESEARCH

Open Access

High Sensing Performance Toward Acetone Vapor Using TiO_2 Flower-Like Nanomaterials

Weiye Yang[1,2,3,4], Quanhong Ou[1,2,3], Xueqian Yan[1,2,3], Lei Liu[1,2,3], Shaoyu Liu[1,2,3], Huohuo Chen[1,2,3] and Yingkai Liu[1,2,3*]

Abstract

For real-application gas sensors, high performances (response, selectivity, response/recovery time and stability) are demanded. An effective strategy is applying nanomaterials in gas sensors. In this study, the anatase TiO_2 flower-like nanomaterials (FLNMs) are prepared through a one-step hydrothermal method which exhibit high-performance toward acetone vapor. TiO_2 FLNMs sensors property are characterized at optimal working temperature of 330 °C with selectivity (acetone), response ($S = 33.72$ toward 250 ppm acetone), linear dependence ($R^2 = 0.9913$), response/recovery time (46/24 s toward 250 ppm acetone) and long-term stability (30 days). These demonstrate that TiO_2 FLNMs get a high performance for acetone sensor. Moreover, the limit of detection of acetone is 0.65 ppm which is lower than that of exhaled air for diabetes (0.8 ppm), indicating that TiO_2 FLNMs gas sensor gets potential application in medical diagnosis.

Keywords: Flower-like TiO_2, Hydrothermal method, Acetone, Gas sensing, Medical diagnosis

Introduction

Over the last couple of decades, due to tremendous requirements for application in plenty of fields such as industrial security and medical diagnosis environmental protection, gas sensors have attracted enthusiastic interest in academic circle [1, 2]. Acetone is a universally used raw material, which is transparent and colorless volatile organic chemical contained with distinct taste and smell, cleanser and diluent in laboratories and industrial manufacture. It is needed to monitor colorless volatile organic concentrations in the workplace for safety and environment for health owing to their explosive possibility and toxicity [3]. Symptoms such as light-headedness and fatigue may be caused by exposure to a certain concentration of acetone (500–2000 ppm). While the concentrations of acetone arise over 2000 ppm, it can give rise to coma, muscle weakness, nausea and even death [4, 5]. Furthermore, acetone concentration in exhaled air is an important indicator of diabetes [6, 7]. It is reported that the concentration of acetone in exhaled air is higher than 1.8 ppm for diabetic, while it is lower than 0.8 ppm for able-bodied person [8]. Therefore, low concentration detection of acetone is significant for diabetes diagnosis.

Metal oxide semiconductors (MOSs) exhibit outstanding sensing performance due to the plentiful oxygen vacancies, which can be beneficial to gas adsorption. Among the MOSs, titanium dioxide (TiO_2) is a widely researched n-type MOSs, which has been used in numerous areas such as solar cells [9], electrochemistry [10, 11], photocatalysis [12] and gas sensors [13]. Various kinds of TiO_2 nanostructures with distinct morphologies and sizes, such as nanowires, nanotubes, nanoparticles and nanobelts have been applied for acetone detecting and displayed high sensing properties [14, 15], whereas several shortcomings like poor stability, low selectivity, low response and long response/recovery times, restricted TiO_2 nanomaterials in realistic application. To conquer these drawbacks, strategies such as core–shell structures

*Correspondence: liuyingkai99@163.com

[1] Yunnan Key Laboratory of Opto-Electronic Information Technology, Yunnan Normal University, Kunming 650500, China
Full list of author information is available at the end of the article

[16], doping [17], functionalize with noble metals [18] and light activation [19] have been demonstrated.

Inspired by these, TiO_2 flower-like nanomaterials (FLNMs) are successfully prepared through a one-step hydrothermal method, which exhibit high sensing performance for acetone. The TiO_2 FLNMs' morphology, crystal structure and elementary composition are analyzed by scanning electron microscope (SEM), transmission electron microscopy (TEM), X-ray diffraction (XRD) and X-ray photoelectron spectroscopy (XPS), respectively. Moreover, the gas properties are well researched and sensing mechanism has also been discussed. These results reveal that TiO_2 FLNMs display greatly response, stability and response properties to the acetone. TiO_2 FLNMs shows a high performance in detecting low concentration acetone, which can be used for diabetes diagnosis.

Experimental Section

Materials

Titanium films (99.999% purity) are bought from Haiyuan Aluminum Corporation, hydrofluoric acid (HF, 40 wt%) is supplied by Tianjin Chemical Reagent Corporation. Acetone (C_3H_6O, 99.5%), ethanol absolute (C_2H_6O, 99.7%), benzene (C_6H_6, 99.5%), toluene (C_6H5CH_3, 99.5%), xylene (C_8H_{10}, 99.0%), methanol (CH_3OH, 99.5%) and formaldehyde solution (HCHO, 37–40%) are bought from Tianjin Chemical Reagent Corporation. All experimental water is deionized water (18.2 MΩ) in this work. All reagents are purchased without any further purification.

Sample Preparation

TiO_2 FLNMs are prepared through a one-step hydrothermal reaction between titanium films and HF, which is mentioned in previous report [20, 21]. Firstly, titanium films (3 cm × 1 cm) are treated by a basic procedure of decontamination. Secondly, titanium films and 10 mmol HF 60 mL are placed to a 100-mL Teflon autoclave, maintaining at the temperature of 110 °C for 6 h. The reaction occurs only on the surface of the titanium film, gray precipitates are scratched off and collected after the autoclave cooling down to room temperature, the final products are washed alternately with absolute ethanol and deionized water for three times. Finally, the specimens are dried at 80 °C and the pure TiO_2 FLNMs powder is obtained. The mechanism of the formation of titania processes is as follows.

$$Ti + 6HF \rightarrow H_2TiF_6 + 2H_2 \uparrow \quad (1)$$

$$H_2TiF_6 + 4H_2O \rightarrow Ti(OH)_4 + 6HF \quad (2)$$

$$Ti(OH)_4 \rightarrow TiO_2 + 2H_2O \quad (3)$$

Characterizations

The surface morphologies are obtained by scanning electron microscope with an acceleration voltage of 30.0 kV (SEM, Quanta FEG 250, FEI, USA). Transmission electron microscopy (TEM) is observed on a JEM-2100 electron microscope. The crystalline phase of all the specimens is identified by the X-ray diffraction analysis with Cu-Kα1 radiation ($\lambda = 1.5405$ Å) scanning from 20° to 80° (XRD, DX-1000, Dandong Fangyuan Instrument Co. Ltd., China). X-ray photoelectron spectroscopy (XPS) is measured to reveal chemical valence states and chemical composition, it was performed on an imaging photoelectron spectrometer (Thermo Fisher Scientific, USA) with a monochromatic Al Kα X-ray source. The gas sensing properties are accomplished by CGS-1TP intelligent gas sensing analysis system (Beijing Elite Tech Co., Ltd. China).

Sensor Preparation

The gas sensors are made by a brush-coating technique. Firstly, TiO_2 FLNMs powder is mixed with deionized water to create a uniform slurry after grinding. Secondly, the paste is coated onto Ag interdigitated electrodes by a paint brush. To increase the stability and repeatability, the prepared sensors are aged at 330 °C for 12 h in ambient air. The related preparation process is displayed in Fig. 1.

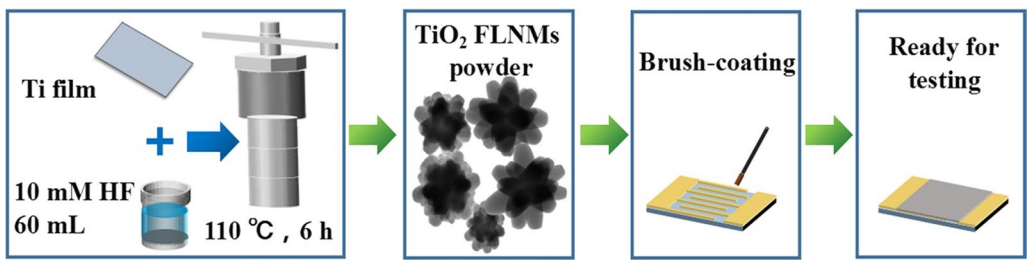

Fig. 1 The schematic diagram of TiO_2 FLNMs sensor preparation and test

The gas sensing measurement are achieved via CGS-1TP intelligent gas sensing analysis system. The microsyringe with the different target liquids is injected into the testing chamber (18 L). Target liquids evaporate into vapor in the chamber. The resistances of TiO_2 FLNMs sensors change rapidly and reach into a steady value. Then, the air is pumped into testing chamber to restore the sensor resistance to its pretest value. The gas sensor response is defined as $S = R_a/R_g$, which R_g and R_a is the resistance under target gas and atmosphere, respectively. The response time/recovery time is defined as the time needed to reach 90% of the saturation S value change upon the target gas or ambient air, respectively.

Results and Discussion

Characterization

The surface morphologies and microstructures of TiO_2 FLNMs are observed by SEM and TEM. SEM images are revealed in Fig. 2a, b. It is evident that TiO_2 composed of aggregated nanoflowers with size around 0.9–1.7 μm. In order to conform insight of TiO_2 FLNMs' microstructures, TEM image is displayed in Fig. 2c. The image exhibits obvious flower-like nanostructure. The crystalline structure of TiO_2 FLNMs is further demonstrated by high-resolution TEM (HRTEM), as shown in Fig. 2d. The lattice space is 0.35 nm which is well matched with the anatase TiO_2 (101).

The crystal structure of TiO_2 FLNMs is also confirmed by XRD, which is portrayed in Fig. 3. It is revealed that the characteristic diffraction peaks is anatase TiO_2 match with the standard data (JCPDS. 21-1272). The composition phase located at 2θ of 25.3°, 37.9°, 48.1°, 54.0°, 55.1°, 62.8°, 68.9°, 70.3° and 75.1° are assigned to (101), (004), (200), (105), (211), (204), (116), (220) and (215) planes of anatase phase.

XPS analysis is applied to confirm the surface elemental chemical states and elementary compositions. Figure 4a shows the full-scale XPS survey scan spectra. It reveals that TiO_2 FLNMs compose of Ti, O and F

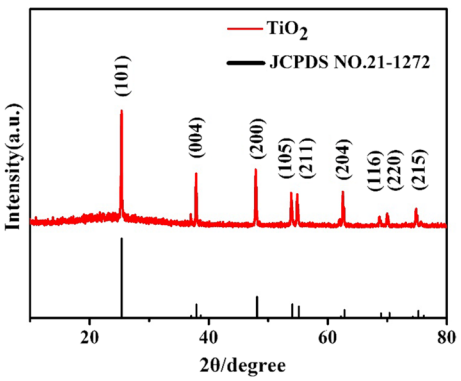

Fig. 3 XRD pattern of TiO2 FLNMs

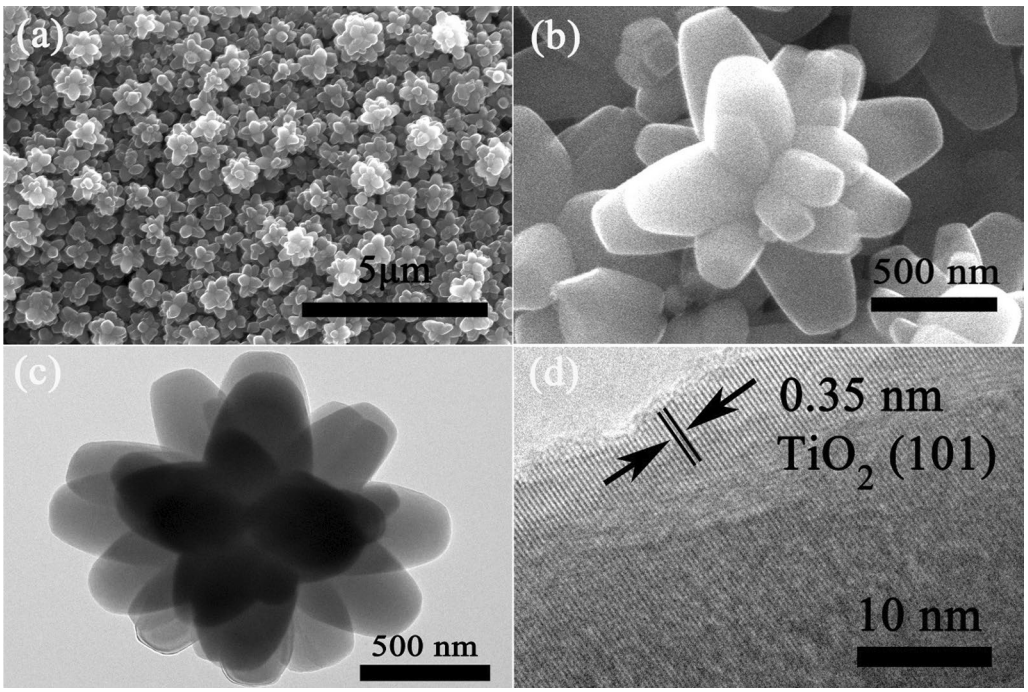

Fig. 2 **a**, **b** SEM images of TiO_2 FLNMs at low and high magnifications, respectively; **c** TEM image of TiO_2 FLNMs; **d** HRETM image

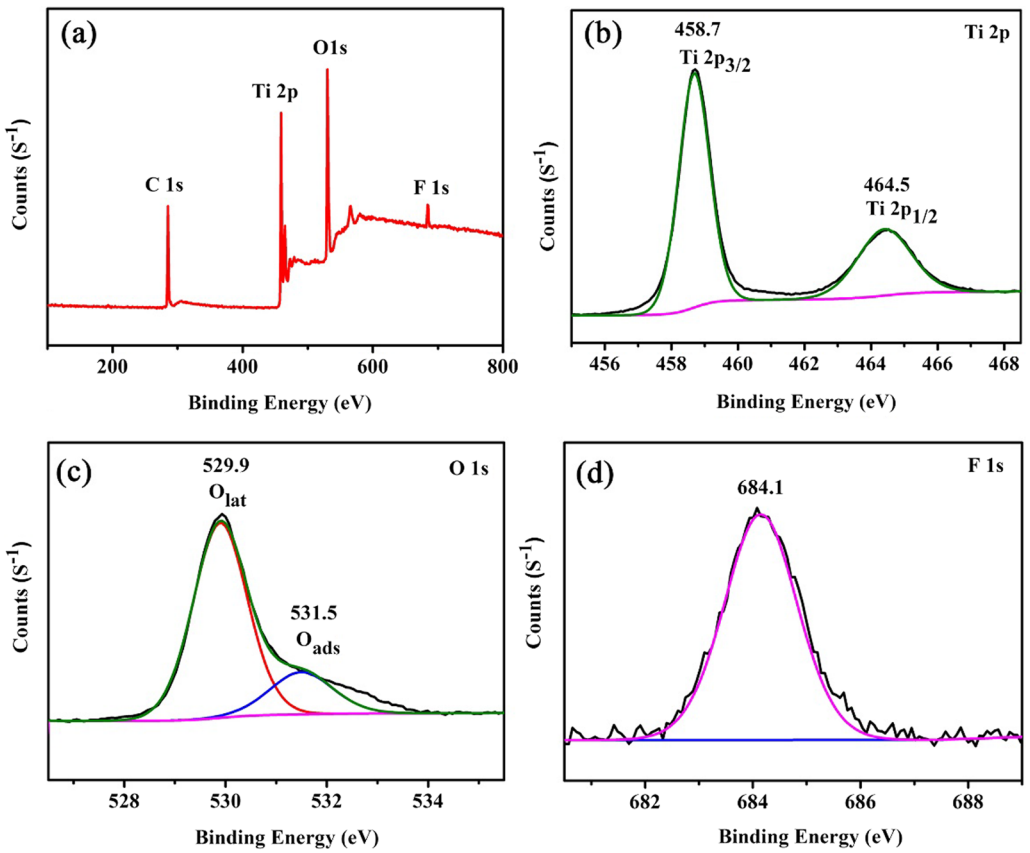

Fig. 4 XPS analysis of TiO2 FLNMs: **a** the full XPS spectrum, **b** Ti 2*p* spectrum, **c** O1*s* spectrum, **d** F 1*s* spectrum

elements, indicating that there are no other impurities, F element is the residual of HF originating from synthetic process. C 1*s* at 284.8 eV is used to the calibration peak. The peaks centered at 458.7 eV and 464.5 eV are corresponding to the spin–orbit split lines of Ti^{4+} $2p_{3/2}$ and Ti^{4+} $2p_{1/2}$, respectively. (Fig. 4b) [22, 23] Fig. 4c displays peaks around at 529.9 eV and 531.5 eV can be assigned to crystal lattice oxygen ions (O_{lat}) and surface adsorbed oxygen ions (O_{ads}). The adsorbed oxygen ions play a significant role in gas sensing property [24–26]. Figure 4d reveals a peak at 684.1 eV which is derived from the adsorbed F on the TiO_2 surface [27].

It is seen from Fig. 5a that the TiO_2 FLNMs has a strong absorption in the range of 300–400 nm with absorption edge of 400 nm. Its band gap is calculated by the following equation.

$$\alpha h\nu = A\left(h\nu - E_g\right)^2 \tag{4}$$

The band gap (*Eg*) of the TiO_2 FLNMs is 3.10 eV, being smaller than that of anatase (3.20 eV), as shown in Fig. 5b. It is reported that F residual have an effect on band gap. It is beneficial to reduce the band gap, facilitate electron transition and improve material properties [28, 29].

Acetone Sensing Properties

To assess applicability of TiO_2 FLNMs sensor for acetone, some fundamental parameters are studied. As we all know, the working temperature is a significant parameter for gas sensors owning to its vigorously affect surface reaction and chemisorption between oxygen and target gas molecules. The most excellent response can be reached at an optimum working temperature when the absorption/desorption achieve equilibrium. To find the optimal working temperature, TiO_2 FLNMs gas sensors are tested under temperatures range from 280 to 440 °C with a concentration of 250 ppm acetone ambient, while the gas sensor prepared with Degussa P25 is also tested at the same condition, as shown in Fig. 6a. It is clearly that the optimal working temperature of TiO2 FLNMs and Degussa P25 both are 330 °C. Thus, all the subsequent experiments are carried out at the optimal working temperature of 330 °C. Furthermore, response

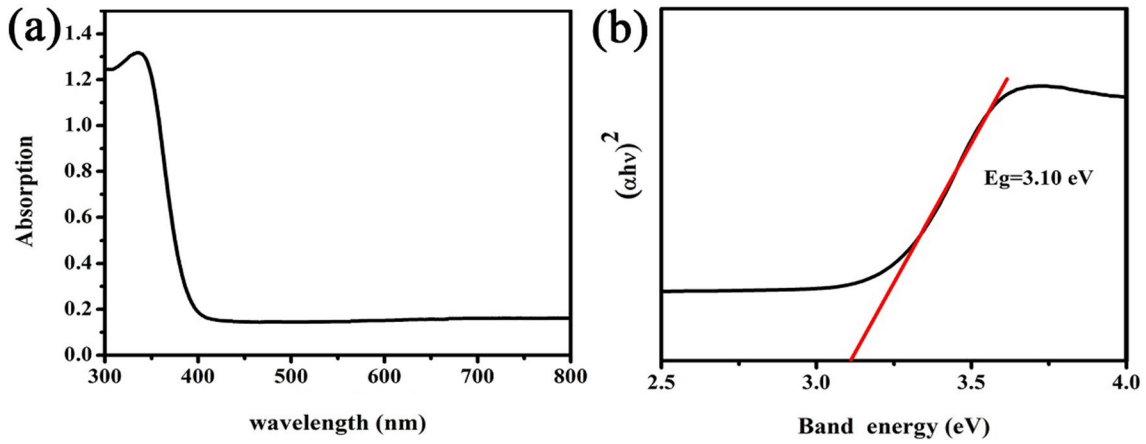

Fig. 5 **a** UV–vis adsorption spectrum of TiO_2 FLNMs; **b** relationship between $(\alpha h\nu)^2 \sim h\nu$

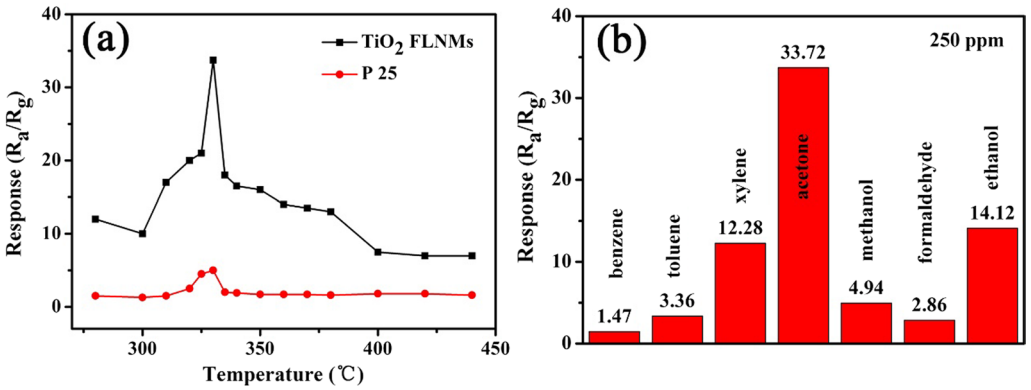

Fig. 6 **a** Response of TiO_2 FLNMs an Degussa P25 powder toward 250 ppm acetone at different operating temperature; **b** selectivity test of TiO_2 FLNMs gas sensor (250 ppm)

of Degussa P25 gas sensors is apparently lower-ranking to TiO_2 FLNMs gas sensor, whereas its response only can achieve 5.0 for 250 ppm acetone and the response of TiO_2 FLNMs is 33.72 in the same circumstance. It indicates that TiO_2 FLNMs show better gas sensing property than commercial Degussa P25. Selectivity represents anti-interference capability to special gases. Thus, the selectivity of TiO_2 FLNMs is analyzed through exposing to 250 ppm benzene, toluene, xylene, acetone, methanol, formaldehyde and ethanol under optimum working temperature, respectively, as revealed in Fig. 6b. It is clearly displayed that the response toward benzene, toluene, xylene, methanol, formaldehyde and ethanol (1.47, 3.36, 12.28, 4.94, 2.86 and 14.12) is much lower than that of acetone (33.72). It indicates that TiO_2 FLNMs sensor shows comparatively selectivity for acetone.

The dynamic response–recover curves of TiO_2 FLNMs sensors versus concentration from 10 to 1000 ppm of acetone and ambient air at optimal working temperature are displayed in Fig. 7a. It is revealed that response is linear relationship in assessing scope. The response of TiO_2 FLNMs linearly increases with the increment of acetone concentration. The linear response dependence on acetone concentration is also studied in Fig. 7b. It shows that the fitting curves versus concentration of acetone toward 10–500 ppm, the correlated coefficients (R^2) is 0.9913 indicating an outstanding linear-dependent relationship between the response and concentration. Another important parameters limit of detection (LOD) are also calculated [30–32]. The LOD of acetone is 0.65 ppm which is lower than the detection limit for diabetes in exhaled air. Therefore, TiO_2 FLNMs gas sensor gets potential application in medical diagnosis.

Repeatability is another significant factor to assess the reliability of the pre-prepared sensor. To evaluate the repeatability of TiO_2 FLNMs sensor, the dynamic sensing toward 250 ppm acetone is measured for 5 cycles (seen in Fig. 7c). It reveals that its response to 250 ppm acetone

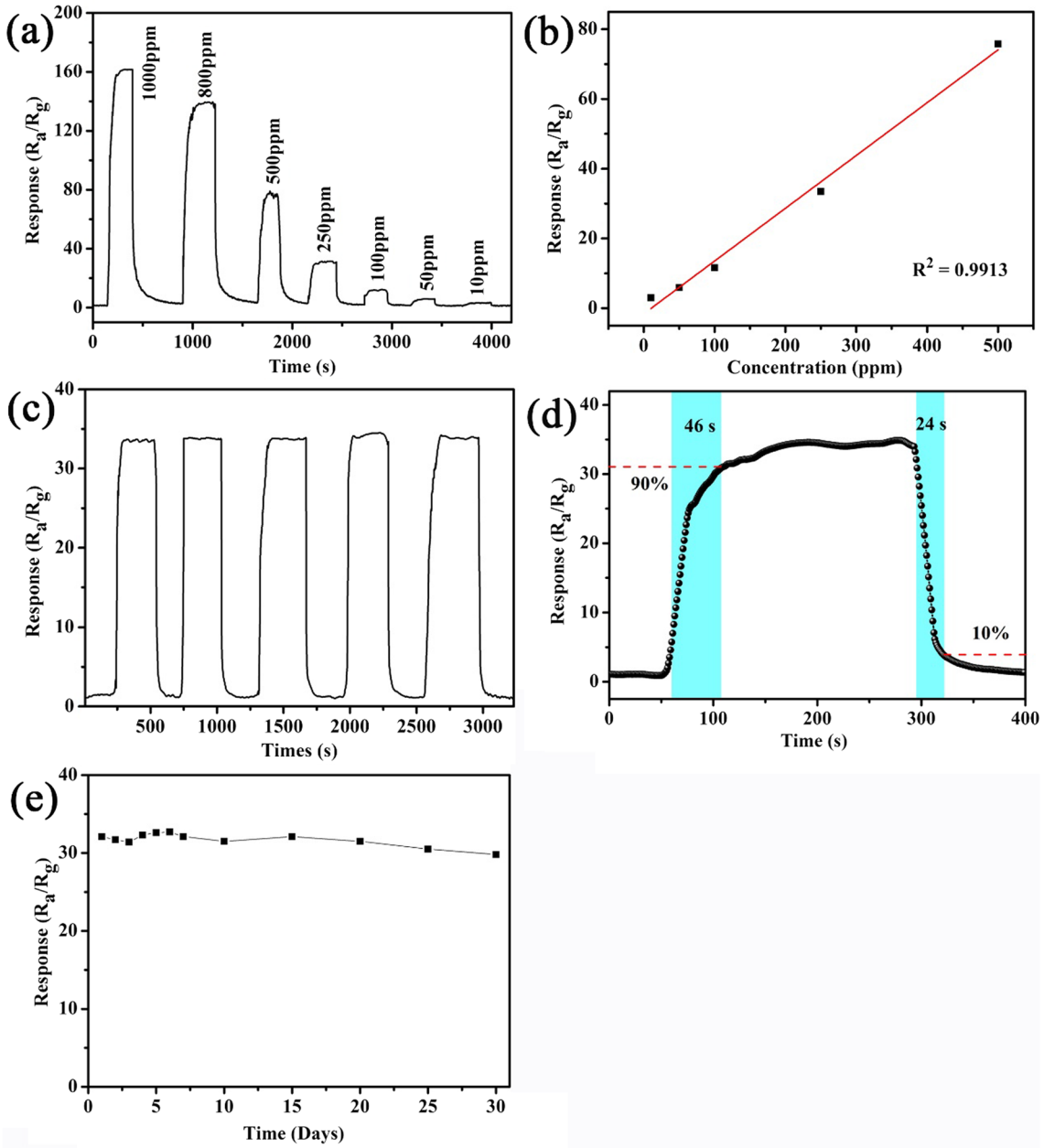

Fig. 7 **a** TiO_2 FLNMs sensing curves versus different concentration (10–1000 ppm) of acetone at 330 °C; **b** the linear response of acetone concentration (10–500 ppm); **c** the reproducibility testing with five cycles; **d** the response/recovery behaviors of TiO_2 FLNMs; **e** the long-term stability test

has no distinct fluctuations, indicating excellent performance of repeatability. Such a high repeatability can be ascribed to the induction of ultra-stable TiO_2 to enhance its sensing stability. Figure 7d displays the response/recovery time of TiO_2 FLNMs. It reveals that the response/recovery time are 46 and 23 s toward 250 ppm acetone, respectively. It indicates that TiO_2 FLNMs sensor exhibits excellent adsorption and desorption property in acetone. This probable reason is that the target molecules are faster and easier dissociated onto the TiO_2 FLNMs' surface, leading to a fast decline in the O^{2-} ions concentration on the surface of TiO2 FLNMs and a rapid increase in the electron concentration, which displays an quick response.

In realistic applications, the long-term stability should be examined. TiO_2 FLNMs gas sensors' response over 30 days

is assessed at the optimal working temperature (seen in Fig. 7e). It illustrates that the responses only have a minor change, which is less than 7.17% of its initial rate. It indicates excellent stability of TiO_2 FLNMs gas sensor. To conform the brilliant sensing performance of TiO_2 FLNMs sensor, a comparison of previous reports and this work on acetone is depicted in Table 1, it further demonstrates that TiO_2 FLNMs represent high acetone sensing performance in this work.

Acetone Sensing Mechanism

TiO_2 is an n-type characteristic semiconductor, while TiO_2 FLNMs sensors are exposed to the acetone vapor, the resistances declined quickly, implying of n-type semiconductor properties. Gas sensing properties rely on the change of surface occupation. As reported by Wolkenstein's model for semiconductors [40], we suggest a correspondent model for TiO_2 FLNMs, as schematically depicted in Fig. 8. In ambient air, oxygen adsorbs onto the surface of TiO_2 FLNMs, and electron transfers from conduction band to the oxygen molecules to create a variety of oxygen ions with distinct valence states (O_{2ads}^-, O_{ads}^-, O^{2-}_{ads}), which gives rise to a thick depletion layer's formation and resulting in a high resistance of the sensor [41, 42]. When TiO_2 FLNMs sensors are exposed to target gas, the reductive gas responds with the oxygen adsorbed on TiO_2 FLNMs surface. The electrons are then freed back to the conduction band of semiconductor, resulting in a lower potential barrier and a thinner depletion layer [43]. This procedure leads to a reduction of resistance and can be expressed by the following equations [35]:

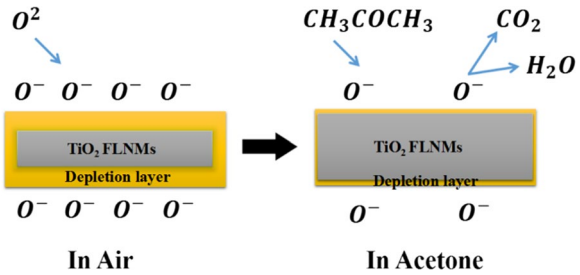

Fig. 8 Sensing mechanism of TiO_2 FLNMs toward ambient air and acetone gas

$$O_2(\text{gas}) \leftrightarrow O_2(\text{ads}) \tag{5}$$

$$O_2(\text{ads}) + e^- \leftrightarrow O_2^-(\text{ads}) \tag{6}$$

$$O_2^-(\text{ads}) + e^- \leftrightarrow 2O^-(\text{ads}) \tag{7}$$

$$O^-(\text{ads}) + e^- \leftrightarrow O^{2-}(\text{ads}) \tag{8}$$

$$CH_3COCH_3(\text{gas}) \leftrightarrow CH_3COCH_3(\text{ads}) \tag{9}$$

$$CH_3COCH_3(\text{gas}) + 8O^- \leftrightarrow 3CO_2(\text{gas}) + 3H_2O(\text{gas}) + 8e^- \tag{10}$$

$$CH_3COCH_3(\text{ads}) + 4O_2^-(\text{ads}) \leftrightarrow 3CO_2(\text{gas}) + 3H_2O(\text{gas}) + 4e^- \tag{11}$$

Table 1 Comparison of various TiO_2 nanostructures toward acetone gas sensing performances

Sensing materials	Working temperature (°C)	Concentration (ppm)	Response (R_a/R_g)	Response/recover time (s)	Reference
Nanoporous TiO_2	370	500	25.97	13/8	[25]
TiO_2 nanoparticles	400	200	7.5	240/180	[33]
Nano nanotube	150	1000	2.08	21/38	[34]
TiO_2 nanorods	500	300	13	12/6	[35]
TiO_2 nanoflowers	280	200	~7	< 50/< 100	[36]
Ag-TiO_2 nanobelts	260	500	28.25	6/8	[24]
Ag-TiO_2 nanospheres	350	500	29.1	1/47	[14]
TiO_2 nanoparticles	270	500	9.19	10/9	[37]
TiO_2 microsphere	320	100	6.9	–	[38]
Brookite TiO_2	320	100	2.3	3/183	[39]
TiO_2 FLNMs	330	250	33.72	46/24	This work

Conclusion

In this work, the newly anatase TiO_2 FLNMs are successfully prepared though a one-step hydrothermal method, which are composed of uniformly flower like nanostructure with size around 0.9–1.7 μm. It is found that this nanomaterials enable a high-performance toward acetone. The results show high selectivity and response, great linear dependence, excellent repeatability, good response/recovery time and long-term stability at an optimum temperature of 330 °C. Interestingly, the LOD of acetone is 0.65 ppm which is lower than that of in exhaled air for diabetes. These results demonstrate a great potential for medical diagnosis. This study paves a new way of using TiO_2 FLNMs for acetone sensor.

Acknowledgements
Not applicable.

Author Contributions
YL guided the experiments and revised the manuscript; QO supplied help for SEM measurements; XY and LL supplied help for gas sensing testing; SL and HC supplied help for data analysis; WY performed the design, fabrication a testing of the device, analyzed the data and wrote the paper. All authors read and approved the final manuscript.

Funding
This work was funded by the National Natural Science Foundation of China (Grant No.11764046 and 11764047).

Availability of Data and Materials
All data generated or analyzed during this study are included in this published article.

Declarations

Ethics Approval and Consent to Participate
Not applicable.

Consent for Publication
Not applicable.

Competing interests
The authors declare no competing interests.

Author details
[1]Yunnan Key Laboratory of Opto-Electronic Information Technology, Yunnan Normal University, Kunming 650500, China. [2]Institute of Physics and Electronic Information, Yunnan Normal University, Kunming 650500, China. [3]Key Laboratory of Advanced Technique and Preparation for Renewable Energy Materials, Ministry of Education, Yunnan Normal University, Kunming 650500, China. [4]Zunyi Medical University, Zunyi 563000, China.

Received: 13 April 2022 Accepted: 20 August 2022
Published online: 02 September 2022

References

1. Novikov S, Lebedeva N, Satrapinski A, Walden J, Davydov V, Lebedev A (2016) Graphene based sensor for environmental monitoring of NO_2. Sens Actuators B Chem 236:1054–1060
2. Xing XX, Du LL, Feng DL, Wang C, Yao MS, Huang XH, Zhang SX, Yang DC (2020) Individual gas sensor detecting dual exhaled biomarkers via a temperature modulated n/p semiconducting transition. J Mater Chem A 8(48):26004–26012
3. Wang CC, Weng YC, Chou TC (2007) Acetone sensor using lead foil as working electrode. Sens Actuators B Chem 122(2):591–595
4. Ge WY, Jiao SY, Chang Z, He XM, Li YX (2022) Ultrafast response and high selectivity toward acetone vapor using hierarchical structured TiO_2 nanosheets. ACS Appl Mater Interfaces 12(11):13200–13207
5. Hou X, Liu H, Zhang Y, Jiang M, Yuan L, Shi J, Hou C (2020) Oxygen vacancies enhancing acetone-sensing performance. Mater Today Chem 18:100379
6. Choi SJ, Jang BH, Lee SJ, Min BK, Rothschild A, Kim ID (2014) Selective detection of acetone and hydrogen sulfide for the diagnosis of diabetes and halitosis using SnO_2 nanofibers functionalized with reduced graphene oxide nanosheets. ACS Appl Mater Interfaces 6(4):2588–2597
7. Park S (2017) Acetone gas detection using TiO_2 nanoparticles functionalized In_2O_3 nanowires for diagnosis of diabetes. J Alloys Compd 696:655–662
8. Wei SH, Zhao GY, Du WM, Tian QQ (2016) Synthesis and excellent acetone sensing properties of porous WO_3 nanofibers. Vacuum 124:32–39
9. Nam J, Kim JH, Kim CS, Kwon JD, Jo S (2020) Surface engineering of low-temperature processed mesoporous TiO_2 via oxygen plasma for flexible perovskite solar cells. ACS Appl Mater Interfaces 12(11):12648–12655
10. Cai Y, Wang HE, Huang SZ, Yuen MF, Cai HH, Wang C, Yu Y, Li Y, Zhang WJ, Su BL (2016) Porous TiO_2 urchins for high performance Li-ion battery electrode: facile synthesis, characterization and structural evolution. Electrochim Acta 210:206–214
11. Dong WJ, Wang D, Li XY, Yao Y, Zhao X, Wang Z, Wang HE, Li Y, Chen LH, Qian D, Su BL (2020) Bronze TiO_2 as a cathode host for lithium–sulfur batteries. J Energy Chem 48:259–266
12. Yu J, Godiksen AL, Mamahkel A, Søndergaard-Pedersen F, Rios-Carvajal T, Marks M, Lock N, Rasmussen SB, Iversen BB (2020) Selective catalytic reduction of NO using phase-pure anatase, rutile, and brookite TiO_2 nanocrystals. Inorg Chem 59(20):15324–15334
13. Zhang R, Zhang T, Zhou TT, Wang LL (2018) Rapid sensitive sensing platform based on yolk-shell hybrid hollow sphere for detection of ethanol. Sens Actuators B Chem 256:479–487
14. Cheng XL, Xu YM, Gao S, Zhao H, Huo LH (2011) Ag nanoparticles modified TiO_2 spherical heterostructures with enhanced gas-sensing performance. Sens Actuators B Chem 155(2):716–721
15. Yang M, Huo LH, Zhao H, Gao S, Rong ZM (2009) Electrical properties and acetone-sensing characteristics of $LaNi_{1-x}Ti_xO_3$ perovskite system prepared by amorphous citrate decomposition. Sens Actuators B Chem 143(1):111–118
16. Katoch A, Choi SW, Sun GJ, Kim HW, Kim SS (2014) Mechanism and prominent enhancement of sensing ability to reducing gases in p/n core–shell nanofiber. Nanotechnology 25(17):175501
17. Su J, Zou XX, Zou YC, Li GD, Wang PP, Chen JS (2013) Porous titania with heavily self-doped Ti^{3+} for specific sensing of CO at room temperature. Inorg Chem 52(10):5924–5930
18. Lai HY, Chen CH (2012) Highly sensitive room-temperature CO gas sensors: Pt and Pd nanoparticle-decorated In_2O_3 flower-like nanobundles. J Mater Chem 22(26):13204–13208
19. Alenezi MR, Alshammari AS, Jayawardena KDGI, Beliatis MJ, Henley SJ, Silva SRP (2013) Role of the exposed polar facets in the performance of thermally and UV activated ZnO nanostructured gas sensors. J Phys Chem C 117(34):17850–17858
20. Wu GS, Wang JP, Thomas DF, Chen AC (2008) Synthesis of F-doped flower like TiO_2 nanostructures with high photoelectrochemical activity. Langmuir 24(7):3503–3509
21. Yang WY, Tang JQ, Ou QH, Yan XQ, Liu L, Liu YK (2021) Recyclable Ag-deposited TiO_2 SERS substrate for ultrasensitive malachite green detection. ACS Omega 6(41):27271–27278
22. Yu W, Liu XJ, Pan LK, Li JJ, Liu JY, Zhang J, Li P, Chen C, Sun Z (2014) Enhanced visible light photocatalytic degradation of methylene blue by F-doped TiO_2. Appl Surf Sci 319:107–112
23. Li JJ, Xu XT, Liu XJ, Yu CY, Yan D, Sun Z, Pan LK (2016) Sn doped TiO_2 nanotube with oxygen vacancy for highly efficient visible light photocatalysis. J Alloys Compd 679:454–462
24. Zhu H, Haidry AA, Wang Z, Ji YW (2021) Improved acetone sensing characteristics of TiO_2 nanobelts with Ag modification. J Alloys Compd 887:161312

25. Chen N, Li YX, Deng DY, Liu X, Xing XX, Xiao XC, Wang YD (2017) Acetone sensing performances based on nanoporous TiO_2 synthesized by a facile hydrothermal method. Sens Actuators B Chem 238:491–500
26. Zhang ML, Yuan ZH, Ning T, Song JP, Zheng C (2013) Growth mechanism of Pt modified TiO_2 thick film. Sens Actuators B Chem 176:723–728
27. Yu JC, Yu JG, Ho WK, Jiang ZT, Zhang LZ (2002) Effects of F-doping on the photocatalytic activity and microstructures of nanocrystalline TiO_2 powders. Chem Mater 14(9):3808–3816
28. Serpone N, Lawless D, Khairutdinov R (1995) Size Effects on the photophysical properties of colloidal anatase TiO_2 particles: size quantization versus direct transitions in this indirect semiconductor? J Phys Chem 99(45):16646–166654
29. Zhang JF, Zhou P, Liu JJ, Yu JG (2014) New understanding of the difference of photocatalytic activity among anatase, rutile and brookite TiO_2. Phys Chem Chem Phys 16:20382–20386
30. Dua V, Surwade SP, Ammu S, Agnihotra SR, Jain S, Roberts KE, Park S, Ruoff RS, Manohar SK (2010) All-organic vapor sensor using inkjet-printed reduced graphene oxide. Angew Chem Int Ed 49(12):2154–2157
31. Li J, Lu YJ, Ye Q, Cinke M, Han J, Meyyappan M (2003) Carbon nanotube sensors for gas and organic vapor detection. Nano Lett 3(7):929–933
32. Liu L, Yang WY, Zhang H, Yan XQ, Liu YK (2022) Ultra-high response detection of alcohols based on CdS/MoS_2 composite. Nanoscale Res Lett 17(1):1–10
33. Rella R, Spadavecchia J, Manera MG, Capone S, Taurino A, Martino M, Caricato AP, Tunno T (2007) Acetone and ethanol solid-state gas sensors based on TiO_2 nanoparticles thin film deposited by matrix assisted pulsed laser evaporation. Sens Actuators B Chem 127(2):426–431
34. Bhattacharyya P, Bhowmik B, Fecht HJ (2015) Operating temperature, repeatability and selectivity of TiO_2 nanotube-based acetone sensor: influence of Pd and Ni nanoparticle modifications. IEEE Trans Device Mater Reliab 15(3):376–383
35. Bian HQ, Ma SY, Sun AM, Xu XL, Yang GJ, Gao JM, Zhang ZM, Zhu HB (2015) Characterization and acetone gas sensing properties of electrospun TiO_2 nanorods. Superlattice Microstruct 81:107–113
36. Zhang RG, Liu ZX, Ling LX, Wang BJ (2015) The effect of anatase TiO_2 surface structure on the behavior of ethanol adsorption and its initial dissociation step: a DFT study. Appl Surf Sci 353:150–157
37. Navale ST, Yang ZB, Liu CST, Cao PJ, Patil VB, Ramgir NS, Mane RS, Stadler FJ (2018) Enhanced acetone sensing properties of titanium dioxide nanoparticles with a sub-ppm detection limit. Sens Actuators B Chem 255:1701–1710
38. Yang Y, Liang Y, Wang GZ, Liu LL, Yuan CL, Yu T, Li QL, Zeng FY, Gu G (2015) Enhanced gas-sensing properties of the hierarchical TiO2 hollow microspheres with exposed high-energy 001 crystal facets. ACS Appl Mater Interfaces 7(44):24902–24908
39. Cao S, Sui N, Zhang P, Zhou TT, Tu JC, Zhang T (2022) TiO_2 nanostructures with different crystal phases for sensitive acetone gas sensors. J Colloid Interfaces Sci 607:357–366
40. Drost H (1991) Electronic processes on semiconductor surfaces during chemisorption. Z Phys Chem 177(1):123–123
41. Cao MH, Wang YD, Chen T, Antonietti M, Niederberger M (2008) A highly sensitive and fast-responding ethanol sensor based on $CdIn_2O_4$ nanocrystals synthesized by a nonaqueous sol—gel route. Chem Mater 20(18):5781–5786
42. Liu X, Chen N, Xing XX, Li YX, Xiao XC, Wang YD, Djerdj I (2015) A high-performance n-butanol gas sensor based on ZnO nanoparticles synthesized by a low-temperature solvothermal route. RSC Adv 5(67):54372–54378
43. Liu X, Chen N, Han BQ, Xiao XC, Chen G, Djerdj I, Wang YD (2015) Nanoparticle cluster gas sensor: Pt activated SnO_2 nanoparticles for NH_3 detection with ultrahigh sensitivity. Nanoscale 7(36):14872–14880

Publisher's Note